Nuclear Materials and Energy 37 (2023) 101500

Contents lists available at ScienceDirect

Nuclear Materials and Energy

journal homepage: www.elsevier.com/locate/nme

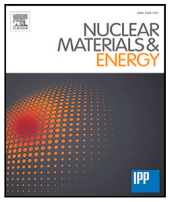

Modelling the PbLi flow including tritium transport and permeation with GETTHEM

Roberto Bonifetto [a,*], Nicolò Abrate [a], Antonio Froio [a], Fabrizio Lisanti [a], Francesca Papa [b], Marco Utili [c], Alessandro Venturini [c]

[a] NEMO Group, Dipartimento Energia, Politecnico di Torino, c.so Duca degli Abruzzi 24, 10129, Torino, Italy
[b] DIAEE Department, Sapienza University of Rome, 00186, Rome, Italy
[c] ENEA – Brasimone, Fusion and Technology for Nuclear Safety and Security Department, 40032, Camugnano (BO), Italy

ARTICLE INFO

Keywords:
EU DEMO
Fusion reactors
PbLi
Permeator against vacuum
Tritium extraction

ABSTRACT

One of the main challenges to be addressed to achieve a reliable electricity production from the EU DEMO reactor is the realization of a closed fuel cycle, for which a suitable Tritium Extraction and Removal System (TERS) is required. One of the possible technologies identified for the EU DEMO TERS is the Permeator Against Vacuum (PAV): the tritium dissolved in the liquid PbLi flowing within several parallel channels will permeate towards the vacuum pumped on the other side of the channel wall (the membrane).

A recently-developed model of the tritium permeation across the membrane in the PAV, involving both transport phenomena in the wall and surface processes, was already used to size the EU DEMO PAV. However, besides the component itself, it is important to properly define the interfaces of the PAV in the TERS, and of the TERS in the entire PbLi and tritium loops. The model of such a complex system is therefore implemented here in the Modelica object-oriented language used by system-level tool GETTHEM, that already includes a model of the PbLi loop. The resulting, lumped-parameter component will be able to capture the thermal-hydraulic behaviour of the PbLi, to model the tritium transport in the fluid and to estimate the tritium permeated flux supplied to the tritium processing. Such a model is tested here on a sub-scale circuit to demonstrate its capability to simulate the operation of the EU DEMO TERS using the GETTHEM code.

As the physical parameters of the model are subject to a large uncertainty, an uncertainty propagation analysis is also performed, to have a preliminary quantification of the impact of such uncertainties on the model output and, therefore, on the TERS efficiency, and to drive further investigations of these physical properties. In particular, results show how the uncertainty on the solubility constant of hydrogen in PbLi represents the dominant contribution on the total variance, highlighting the need for a better accuracy of such parameter.

1. Introduction

Tritium self-sufficiency is one of the challenges on the path towards a reliable electricity production from fusion energy by means of the EU DEMO reactor [1]. Its Breeding Blanket (BB) and Tritium Extraction and Removal System (TERS) must be designed to minimize the tritium inventory. The Test Blanket Module (TBM) programme in ITER will provide a validation of the different designs. Both TBM programme and EU DEMO design require substantial R&D, in turn asking for support from reliable modelling to prepare the experiments and compare different solutions.

One of the BB designs that is being considered for the EU DEMO and is going to be tested in a TBM is the Water Cooled Lithium Lead (WCLL) [2] BB; it adopts water for the cooling and flowing PbLi as a breeder material. The tritium exiting the BB in the PbLi mass flow rate should then be extracted in the TERS to close the fuel cycle, providing it to the Tritium Plant for the subsequent processing stages before being injected in the core plasma as fuel. Among the technologies investigated for the Tritium Extraction Unit (TEU), the one considered for the work presented in this paper is the Permeator Against Vacuum (PAV).

The functioning principle of the PAV technology is based on the tritium transport through a membrane permeable to tritium, which separates the flowing PbLi, where tritium is dissolved, from an outer chamber where vacuum is pumped. The driver for the tritium flux from the PbLi to the vacuum side is the partial pressure difference between the two sides of the membrane. Thanks to this, the PbLi leaves the

* Corresponding author.
E-mail address: roberto.bonifetto@polito.it (R. Bonifetto).

https://doi.org/10.1016/j.nme.2023.101500
Received 9 July 2023; Received in revised form 17 August 2023; Accepted 4 September 2023
Available online 9 September 2023

PAV channels (whose wall is the membrane itself) with a lower tritium concentration.

A conceptual design for the PAV is based on the shell-and-tube configuration with PbLi pipes shaped as U-tubes (see Fig. 1) surrounded by a vessel where vacuum is pumped; it was presented by Politecnico di Torino and ENEA for the WCLL BB [3], exploiting a recently-developed, steady-state, surface-limited model of the tritium permeation through the PAV membrane [4] for the dimensioning of the extractor. Moreover, the PAV conceptual design was adapted for the design of a PAV mock-up tested in TRIEX-II facility at ENEA Brasimone Research Center [5], where the experimental qualification of several TEU options is carried out.

The aim of the present work is to implement a dynamic system-level model for the transport and extraction of Tritium inside the PbLi loop of the WCLL BB, to support the conceptual design of the TEU based on the PAV technology and assess its dynamic behaviour by simulating it during different transients. The new model is implemented in the system-level GEneral Tokamak THErmal-hydraulic Model (GETTHEM) [6,7], a code developed at Politecnico di Torino since 2015 for the thermal-hydraulic modelling of the Breeding Blanket (BB) and related subsystems. Taking advantage of the object-oriented nature of the GETTHEM code, the PbLi loop model, featuring the new permeation model for the PAV, can be easily adapted to reproduce the layout and operative conditions of the TERS PbLi loop of any fusion experiment adopting this technology. Therefore, the adaption of the model to the TRIEX-II facility [8] is foreseen for a future validation against the data obtained during TRIEX-II experimental campaign on the PAV mock-up [9].

Several tools were developed, in the past years, for the modelling of the transport and permeation phenomena of tritium in lead-lithium loops of fusion reactors: for instance, the object-oriented software EcosimPro [10] was used in [11,12] to model the WCLL and Dual-Coolant Lithium-Lead PbLi loops at a system-level, providing a dynamic assessment of tritium inventories in the blanket and related systems; the FUS-TPC code [13], developed with the MATLAB environment and based on the fast-fission SFR-TPC code [14], which was used in [15] to estimate tritium inventories and losses – assuming 0D tritium mass balance in components and diffusion-limited permeation through the channel walls – for the PbLi loops of the WCLL and Helium-Cooled Lithium-Lead BBs. These tools, however, model the tritium extraction in the TEU with a fixed extraction efficiency and, to the best of the authors' knowledge, a system-level model of a Pbli loop implementing a detailed permeation model for the PAV tritium extractor is still missing in literature.

Finally, due to the large uncertainty on the main physical parameters involved in the extraction of the hydrogen isotopes in the PAV, a preliminary uncertainty propagation study is carried out in this work aiming at improving the physical understanding of such parameters, quantifying their mutual dependence and their impact on the PAV outputs, and identifying the main contributors on the overall uncertainty on the outputs.

2. Description of the model

The GETTHEM code is written using the Modelica language, and it is based on the Modelica Standard Library (MSL) and on the ThermoPower library [16]. Its modular structure allows simple modelling of complex systems with a graphical interface, and enables the generation of new models by extending existing objects, thanks to the object-oriented approach.

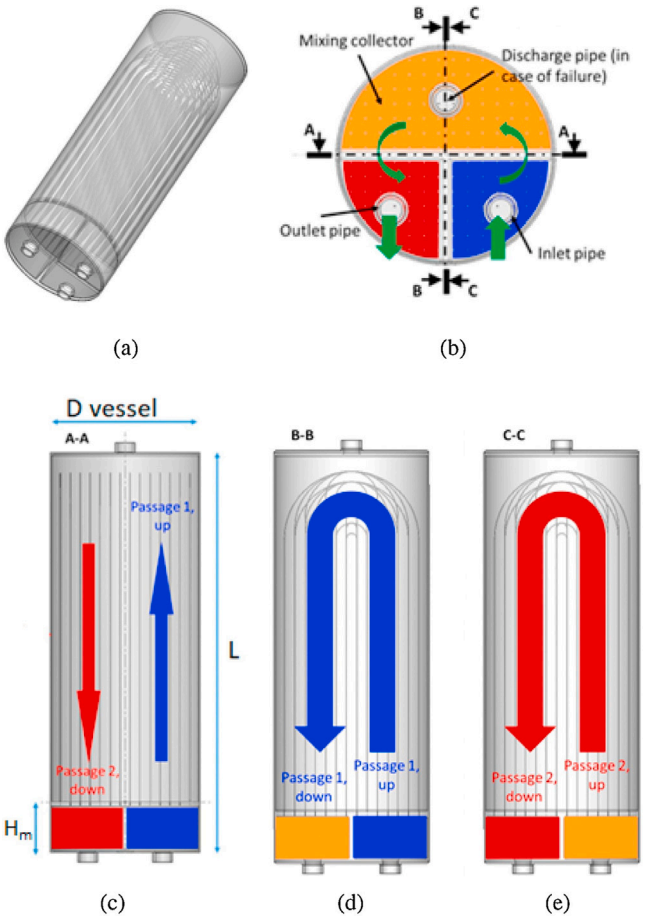

Fig. 1. View of the PAV design proposed in [3]: (a) 3D view, (b) top view of the vessel internals (with the inlet/outlet and discharge pipes in transparency), (c) side view of the vessel internals (with inlet and outlet manifolds) and side view of the passage 1 (d) and passage 2 (e).

2.1. Model assumptions

The transport of tritium is modelled in this work as a scalar transport. In the work presented in [17], a model for the assessment of the generation and transport of activated corrosion products (ACPs) as dispersed materials (DMs) in the WCLL PbLi loop was recently implemented in GETTHEM; such model allows the possibility to include an unlimited number of DMs within the working fluid, PbLi in this case. In the present work, such model has been applied to the transport of tritium (or generically of hydrogen isotopes) as a DM in PbLi, and extended to model also the permeation phenomena through a membrane in the PAV.

The core assumption behind the modelling of the transport of DMs is that the DM particles are found in the fluid in trace concentration only, according to the Modelica.Media definition [18,19], under the assumption that their presence does not significantly affect the fluid properties. In view of the low fluid velocity, the PbLi flow is assumed to be incompressible. Further details on the DM transport model can be found in [17].

Additionally, some assumption for the modelling of the permeation phenomena through the membrane of the PAV have been made, namely [4]:

- the Nb membrane operation is considered at steady state, meaning that the different species involved are in thermodynamic equilibrium, and no accumulation is modelled;

- the entire PAV system (PbLi + membrane) is considered isothermal;
- tritium has the same velocity of the PbLi flow inside the PAV channels;
- the mass diffusion of tritium is driven by partial pressure gradients;
- the PbLi flow is considered to have a fully developed velocity profile in turbulent regime along the entire channel length, thus the tritium concentration is considered uniform across most of the channel cross section;
- the tritium mass transport in the radial direction is driven by the turbulent mixing within the PbLi bulk, the diffusion in the fluid close to the membrane wall and the permeation through the membrane, whereas in the axial direction it is driven by the advection within the PbLi flow; hence, diffusion across the channel prevails with respect to that along the channel, which can be neglected.

From the last two assumptions, it follows that the assessment of the distribution of tritium concentration inside the PAV is carried out through the combination of two 1D models: (i) a 1D tritium flow model along the Pbli flow direction, where the mass balance equation for tritium is solved (see Section 2.2.1), and (ii) a 1D permeation model in the radial direction through the membrane. The model does not assume *a priori* the permeation regime: depending on the operating conditions given by the input parameters, it can address both surface and diffusion limited regimes [4].

2.2. Model equations

The new component for the PAV channels relies on the Modelica.Fluid package available in the MSL [19], which is a free and open source library. As discussed in [17], this approach is compatible with existing GETTHEM models, as all of them are based on the same interfaces.

The new PAV channel component is made of a 1D flow model for the PbLi flow (including the axial and radial transport of tritium in PbLi), a radial permeation model across the Nb membrane and a model for the vacuum boundary condition (see Fig. 2); while the first one is adapted from an existing pipe model of the MSL, the latter two are built from scratch.

Note that in the following description of the model implementation, tritium has been considered as the hydrogen isotope solute in PbLi for the transport and permeation study, since it is the H-isotope of interest for the TERS of the EU DEMO reactor and other future tokamaks; however, the model can be straightforwardly adapted to the transport and permeation of other H isotopes if necessary (for example protium in the case of the PbLi loop of the TRIEX-II facility), with just a few precautions on the input parameters , i.e. using in the model equations the molar mass of the H isotope considered and adopt empirical formulation for the solubility and recombination constants developed for the H isotope of interest (or, if missing for that specific isotope, consider a suitable scaling factor).

2.2.1. Mass transport in the axial direction

The tritium advection within the PbLi flow, similarly to what has been done in [17] for the ACPs, is implemented in the PbLi flow model by solving the 1D mass conservation equation for tritium,

$$A\left(\frac{\partial \rho_T}{\partial t}+\frac{\partial \rho_T v}{\partial x}\right)=s_T \tag{1}$$

where A is the channel cross section, ρ_T is the mass of tritium per unit volume of PbLi (in kg_T/m^3_{PbLi}), t is the time, v is the speed of the working fluid, x is the coordinate representing the 1D flow direction, and s_T is the sink term accounting for tritium permeation through the membrane wall expressed in $kg_T/(m\,s)$.

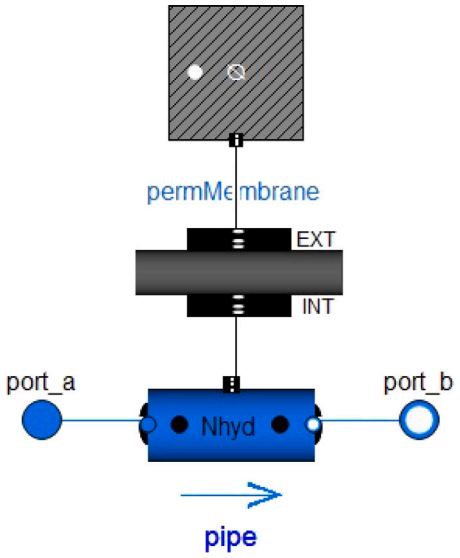

Fig. 2. Sketch of the model of the PAV component implemented in GETTHEM.

The Finite Volume (FV) approach with an upwind scheme is used to approximate the space derivative, splitting the domain in N_V control volumes (CV) of equal length Δx and centroid x_i. Defining the tritium mass concentration $C_T=\frac{M_T}{M}$ (in kg_T/kg_{PbLi}), where M_T is the tritium mass and M is the working fluid mass, and integrating Eq. (1) in space over each CV, the following conservation equation for the tritium mass is found:

$$M\frac{dC_{T,i}}{dt}=\dot{m}_{i,in}(t)C_{T,i,in}(t)-\dot{m}_{i,out}(t)C_{T,i,out}(t)+S_{T,i}(t)\quad \forall i\in[1,N_V] \tag{2}$$

where $\dot{m}_{i,in/out}$ is the working fluid mass flow rate at the ith CV inlet/outlet, $C_{T,i}$ is the concentration in the ith CV, $C_{T,i,in/out}$ is the upstream concentration of tritium at the ith CV boundary (inlet/outlet), and $S_{T,i}(t)=s_T(x_i,t)\Delta x$ is the permeated tritium mass flow rate (in kg/s), which is computed as

$$S_{T,i}=-J_{T,i}\,A_{w,i}\,MM_T\qquad \forall i\in[1,N_V] \tag{3}$$

where $J_{T,i}$ is the tritium mass flux (in $mol/(m^2\,s)$) in the ith CV computed according to the permeation model (see Section 2.2.2), $A_{w,i}$ is the wetted surface of the ith CV and MM_T is the atomic tritium molar mass (in kg_T/mol_T). Further details about the model implementation can be found in [17].

2.2.2. Mass transport in the radial direction

In the past years, some models for the estimation of the tritium permeated flux across a membrane were developed (e.g. that presented in [20], used for a preliminary dimensioning of PAV for the EU DEMO TERS [21], or that in [22], adopted to investigate the use of conventional Reduced Activation Ferritic-Martensitic steels for the membrane as an alternative to Nb) assuming that permeation is predominantly driven by the diffusion inside the membrane. However, despite surface phenomena on the vacuum side were already partially included in [20], it is required to account also for the surface phenomena limiting the tritium permeation on the interface between PbLi and membrane. A new steady-state model including the surface phenomena on the PbLi side was developed in [4], adapting the permeation model in [23] developed for the case of a gaseous carrier to the case of a liquid carrier. In the present work, the permeation model developed in [4] is implemented in the GETTHEM model of the PAV component to compute the tritium mass flux $J_{T,i}$ in Eq. (3).

The tritium concentration is uniform in most of the PbLi channel cross section due to the turbulent mixing, but a localized concentration

gradient is assumed close to the membrane wall, implemented in the PbLi flow model as

$$J_{T,i} = h_T\left(C_{T,i} - C_{T,l,i}\right)\frac{\rho_{PbLi,i}}{MM_T} \qquad \forall i \in [1, N_V] \tag{4}$$

where $C_{T,l,i}$ (expressed in kg_T/kg_{PbLi}) is the tritium concentration close to the membrane, $\rho_{PbLi,i}$ is the PbLi density (in kg_{PbLi}/m^3_{PbLi}) and h_T is the mass transport coefficient (in m/s), which quantifies the rate at which tritium crosses the flow boundary layer. The tritium concentration in PbLi at the membrane interface $C_{T,l,i}$ is computed at each CV i with the Sievert's law, with the assumption of thermodynamic equilibrium

$$C_{T,l,i} = K_{s,i}^{PbLi}\sqrt{p_{T,l,i}}\frac{MM_T}{\rho_{PbLi,i}} \qquad \forall i \in [1, N_V] \tag{5}$$

where $K_{s,i}^{PbLi}$ is the solubility (or Sievert's) constant of tritium in PbLi (computed in the ith CV as a function of the local temperature value), in $mol_T/(m^3_{PbLi}Pa^{1/2})$ and $p_{T,l,i}$ is the tritium partial pressure at the membrane interface, in Pa.

As to the membrane model, the mass diffusion inside the membrane bulk is expressed by the Fick's law, which, given the cylindrical geometry of the system, becomes

$$J_{T,i} = D_{Nb,i}\frac{\widetilde{C}_{T,w,in,i} - \widetilde{C}_{T,w,out,i}}{r_{in}\log\left(\frac{r_{out}}{r_{in}}\right)} \qquad \forall i \in [1, N_V] \tag{6}$$

where $D_{Nb,i}$ is the mass diffusion coefficient (or diffusivity) in Nb (in m^2/s), $\widetilde{C}_{T,w,in}$ and $\widetilde{C}_{T,w,out}$ are the concentrations[1] close to the inner and outer surfaces, respectively, in mol/m^3. On the inner and outer surfaces of the membrane, the mass transport is the result of recombination and dissociation processes, described in [24]. Therefore, the recombination mass flux $J_{T,r,i}$ and the dissociation mass flux $J_{T,d,i}$, having opposite directions, contribute to the total mass flux across the surfaces, which is computed for the ith CV at the inner surface as

$$J_{T,i} = K_{d,i}^{Nb}p_{T,l,i} - K_{r,i}^{Nb}\widetilde{C}^2_{T,w,in,i} \qquad \forall i \in [1, N_V] \tag{7}$$

and at the outer surface as

$$J_{T,i} = 2\frac{r_{out}}{r_{in}}K_{r,i}^{Nb}\widetilde{C}^2_{T,w,out,i} - \frac{1}{2}\frac{r_{out}}{r_{in}}K_{d,i}^{Nb}p_{vc} \qquad \forall i \in [1, N_V] \tag{8}$$

where $K_{d,i}^{Nb}$ is the dissociation constant in $mol_T/(m^2\,s\,Pa)$, given by the product $K_{d,i}^{Nb} = K_{r,i}^{Nb}\left(K_{s,i}^{Nb}\right)^2$ if the thermodynamic equilibrium is assumed, and p_{vc} is the counter-pressure on the vacuum side (different from 0, realistically), assumed uniform along the channel length. $K_{r,i}^{Nb}$ and $K_{s,i}^{Nb}$ are the recombination (in $m^4/(mol_T\,s)$) and solubility (in $mol_T/(m^3\,Pa^{1/2})$) constants in the Nb membrane, respectively. The surface kinetic at the PbLi side is not strictly required as the tritium is dissolved in PbLi as atoms rather than molecules. However, it is considered here to try and account for the possible oxidation of the surface; actually, here a gas-boundary layer of negligible thickness is considered, allowing to account for the surface kinetic. Note that the variables $J_{T,i}$ appearing in Eqs. (4), (6), (7) and (8) are the same quantity, that is the tritium mass flux in the radial direction. The implementation of this model has been successfully verified with the method of manufactured solution, as reported in the Appendix.

3. Test cases

The PbLi loop is one of the ancillary systems of those BB concepts adopting liquid PbLi eutectic alloy as tritium breeder and neutron multiplier (e.g. the WCLL); it consists of a closed circuit where forced circulation of the PbLi eutectic alloy is provided to ensure and maintain

[1] Note that the symbol C is used for a concentration expressed in kg_T/kg_{PbLi}, whereas the symbol $\widetilde{C}$ is used for a concentration expressed in mol/m^3, i.e. at any location $\mathbf{x}$, $\widetilde{C}(\mathbf{x}) = C(\mathbf{x})\frac{\rho_{solvent}(\mathbf{x})}{MM_T}$.

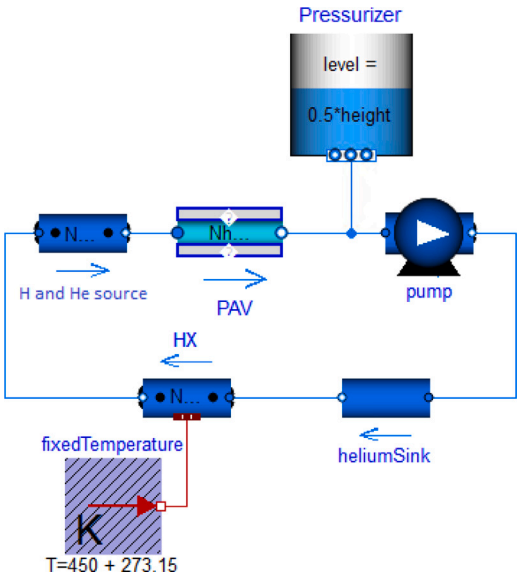

Fig. 3. Scheme of the PbLi loop model for test case I and II ; for test case I, since the He source is equal to zero, the helium sink model is not included in the circuit.

suitable operating conditions for the BB regular operation. Other important functions of this system are: (i) to allow the extraction of the tritium produced inside the blanket, (ii) to remove impurities (e.g. ACPs) from the PbLi alloy, and (iii) to allow the confinement of radioactive products.

The main aim of this work is to showcase the capability of the code to estimate the tritium mass extracted in the PAV (and hence to estimate its efficiency) and compute the tritium distribution along the PbLi loop, rather than providing final results (for which the needed input are not available at the current status of the design). In view the above, a simple test case for the PbLi loop has been developed, including only a small set of essential components that are needed for the circulation of the PbLi alloy and for the hydrogen isotopes generation, transport and extraction. In this test case, protium has been considered as the H-isotope dissolved in the working fluid. The resulting model for this test case (from now on called test case I), shown in Fig. 3, features the following components:

- H-isotopes source, mimicking the function of the breeding units in the EU DEMO BB;
- PAV;
- Pressurizer;
- Pump;
- Heat eXchanger (HX).

The objects adopted for the pump, the HX and the pressurizer are available within MSL: the pump object models a centrifugal pump with ideally controlled mass flow rate, the HX, assumed to be ideal, is modelled by a simple 1D flow model without any wall and with a fixed temperature boundary condition at the secondary side, and the pressurizer is modelled as a pressurized tank.

For the hydrogen isotope source model, instead, an existing pipe model, available within the MSL, is extended to include a hydrogen isotope mass flow source in the working fluid mass balance equation, to be provided as an external input.

The PAV object follows the configuration of the mock-up described in [3] and [5] for a shell-and-tube vessel with 16 niobium U-tubes, modelled as described in Section 2. The Pbli flows through the PAV along 8 parallel channels for each of the two passages inside the component. The geometrical parameters used for the Nb pipes are listed in Table 1. A critical aspect, that must be taken into account for a future

Table 1
Input parameters of the components.

PAV		
Number of parallel channels per passage	8	–
Average channel length	1.888	m
Channel inner diameter	9.2	mm
Channel outer diameter	10	mm
H-isotope source		
Channel length	0.431	mm
Channel diameter	122	mm
H-isotope mass flow source (nominal value)	12	μg/s
Pump		
Nominal rotational speed	1200	rpm
Nominal head	1	bar
Nominal fluid density	9659.8	kg/m^3
Heat exchanger		
Channel length	2	m
Channel diameter	122	mm
Fixed temperature B.C.	450	°C
Pressurizer		
Height	2.11	m
Initial level	1.05	m
Surface pressure	1.0132	bar
Initial and nominal conditions		
H-isotope solute in PbLi	Protium	–
H-isotope initial concentration	0	kg_H/kg_{PbLi}
Nominal mass flow rate	3	kg/s
Nominal pressure	5	bar
Nominal temperature	450	°C

Table 2
Correlations adopted here for the permeation parameters.

Parameter	Expression	Ref.
K_s^{PbLi} [mol/(m^3 Pa$^{1/2}$)]	$4.7 \cdot 10^{-7} \exp(-9000/RT) \frac{\rho_{PbLi}}{MM_{PbLi}}$	[26]
K_s^{Nb} [mol/(m^3 Pa$^{1/2}$)]	$K_{S0} \exp(5550/T)$	[27]
K_r [m^4/(mol s)]	$\frac{1.3 \cdot 10^{24}}{N_A \cdot K_{S0}^2 \cdot \sqrt{T}} \exp\left(\frac{2(E_S - E_C)}{RT}\right)$	[20]
h_T [m/s]	$Sh = 0.0096 Re^{0.913} Sc^{0.346}$	[28]

In the equations above, R is the universal gas constant, T is the temperature (in K), N_A is the Avogadro constant, ρ_{PbLi} is the PbLi density, MM_{PbLi} is the molar mass of PbLi, K_{S0} is the pre-exponential coefficient of the solubility constant (equal to 0.127 mol$_T$/(m^3 Pa$^{1/2}$)), E_S is the heat of solution of tritium in PbLi (equal to −34 kJ/mol [29]) and E_C is the activation energy for dissociative adsorption (equal to 40 kJ/mol [29]).

validation of the model against experimental data, concerns the huge uncertainty on the input parameters used for the permeation model, especially on the solubility constants K_s in PbLi and in Nb, the recombination constant K_r and the mass transport coefficient h_T. As a matter of fact, different empirical formulations available for each of these parameters may give results that differ by several orders of magnitude, as shown in [25] for K_s^{PbLi}. In view of this, a preliminary uncertainty propagation analysis has been performed to assess the effects on the computed PAV efficiency, which is reported in Section 5. Table 2 lists the correlations used for the permeation parameters; for h_T, the correlation is given in terms of the Sherwood dimensionless number Sh

$$Sh = \frac{h_T d}{D} \tag{9}$$

where d is the channel hydraulic diameter and D is the mass diffusion coefficient *in the working fluid*. Sh expresses the ratio of convective to diffusive mass transfer, and it is usually expressed in terms of the Reynolds number Re and of the Schmidt number Sc, in turn defined as the ratio between the kinematic viscosity (momentum diffusivity) ν and D.

Additionally, a second test case (test case II) has been built including also the transport of helium, produced in the BB as a byproduct of

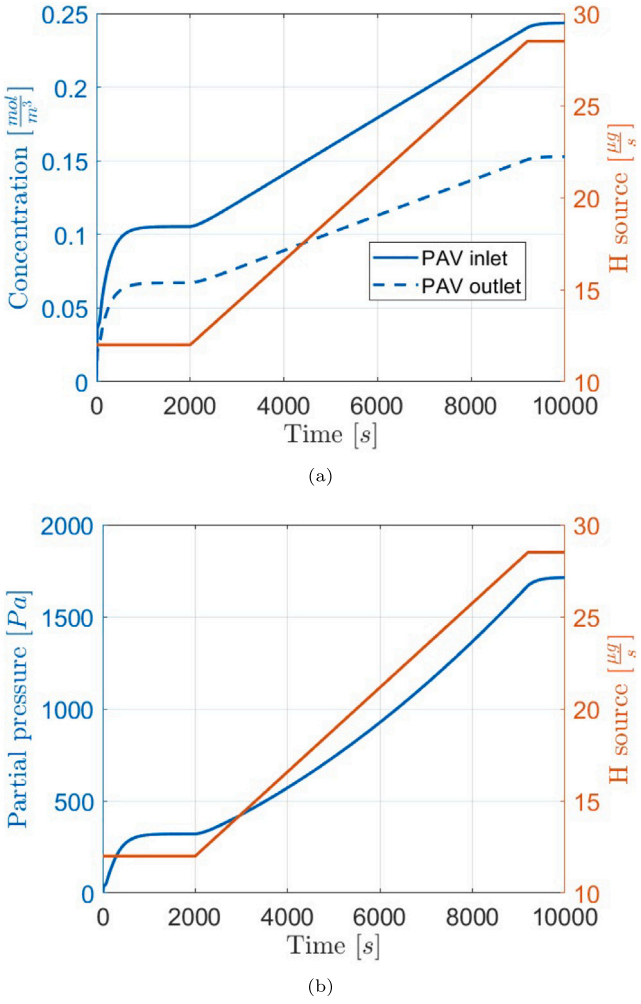

Fig. 4. Test case I: results of the simulations (blue lines, left axis) and evolution of the protium mass source (red line, right axis) for transient Ia: (a) evolution of the protium concentration at the PAV inlet and outlet, and (b) evolution of the protium partial pressure at the PAV inlet.

nuclear reactions between neutrons – coming from the plasma – and Li atoms within the flowing PbLi alloy, to demonstrate the capability of the model to assess the transport of different species inside the loop at the same time. The new test case model, shown in Fig. 3, is almost identical to the previous one, except for:

- the addition of a He mass flow source term in the H-isotope source component ("H and He source" in Fig. 3), and
- the inclusion in the loop of a new model for the He sink, modelled as a simple 0D pipe implementing a fixed He-removal efficiency $\eta = 70\%$.

4. Results

Since the simulation has been performed using 400 CVs (corresponding to a Δx of $\sim$ 0.17 mm) for the spatial discretization of the PAV channel model (for both test cases), the computed values of protium concentration are affected by a relative error of $\sim 10^{-5}$, as computed by the OoA test described in Appendix.

The model adopted for the test case I (see Fig. 3) is run to simulate two possible transients, both starting from a hydrogen isotope concentration in the PbLi equal to zero.

For the first transient (hereafter referred to as transient Ia), the protium mass source is switched on at time $t = 0$ s at its nominal value (see

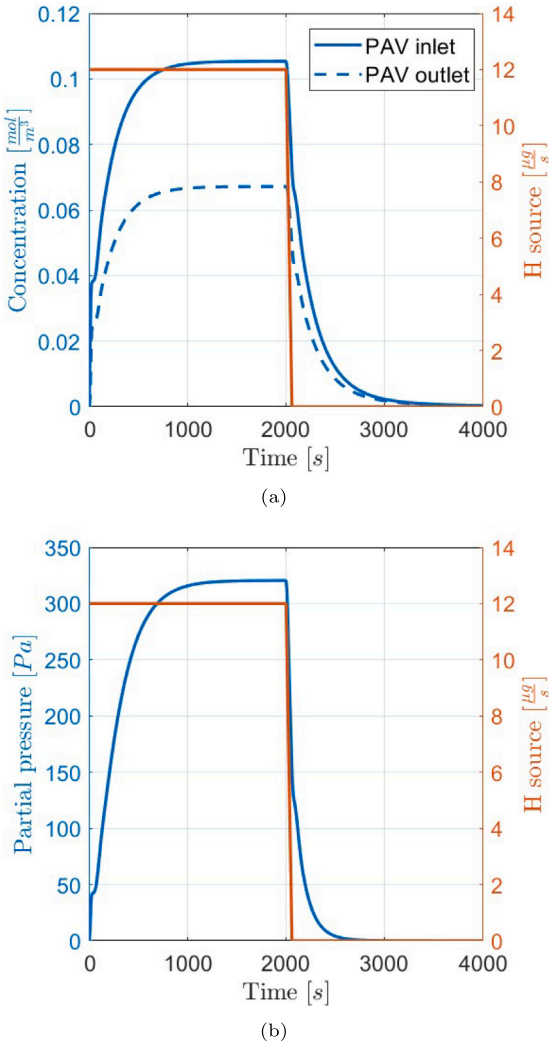

Fig. 5. Test case I: results of the simulations (blue lines, left axis) and evolution of the protium mass source (red lines, right axis) for the transient Ib: (a) evolution of the protium concentration at the PAV inlet and outlet, and (b) evolution of the protium partial pressure at the PAV inlet.

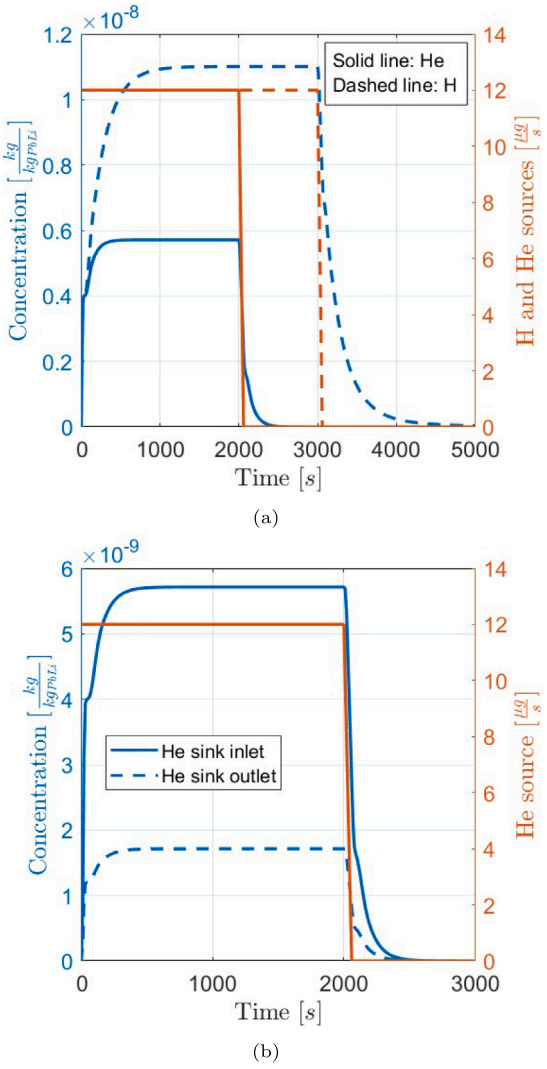

Fig. 6. Test case II: (a) evolution of the protium and helium concentrations at the mass source component outlet (blue lines, left axis), and (b) evolution of the helium concentration at the He sink inlet and outlet (blue lines, left axis). Evolution of He and H mass sources (red lines, right axis) are shown.

Table 1) and kept constant for the first 2000 s of the simulation, during which the system reaches the steady state. At this point, the mass source is continuously increased for 2 hours up to the value of 28.5 μg/s of protium. At the end of the simulation ($t = 10\,000$ s) a new steady state condition is reached. The results for transient Ia are shown in Fig. 4, together with the corresponding waveform of the H mass source. As expected, from Fig. 4(a) it can be seen how the protium concentration at the PAV outlet is lower than that at the inlet, as a mass flux from the PbLi towards the vacuum boundary is established in the extractor; at the final steady state, the PAV efficiency, computed as $\eta = 1 - \frac{C_{PAV,out}}{C_{PAV,in}}$, is 37.2 %. In Fig. 4(b) the partial pressure at the PAV inlet is shown, ranging between the two steady state conditions from ~ 300 Pa up to ~ 1700 Pa.

The transient Ib is identical to the transient Ia up to the end of the first steady state condition. At $t = 2000$ s the protium mass source is switched off within 1 min: most of the protium present inside the PbLi loop is removed by the PAV within approximately 30 min, and the partial pressure at the PAV inlet drops to ~ 0.01 Pa, as shown in Fig. 5.

Concerning the test case II, the model is run for 5000 s to simulate a transient for both protium and helium concentrations, equal to zero at $t = 0$ s. Both the mass sources are switched on and kept constant at their nominal value (for helium, it is assumed as equal to the protium one), reaching the steady state condition, and then shut down at different times. The resulting evolution of the concentration for both species is shown in Fig. 6(a), while the He extraction is reported in Fig. 6(b). The aim of this test case is to display the capability of the model to capture the dynamic evolution of the concentration for different species at the same time, and thus the helium mass source value has been suitably chosen to allow a comparison with the protium concentration, not to provide a realistic estimation on the He inventory in the PbLi loop.

5. A preliminary uncertainty propagation study

The uncertainty affecting a physical parameter is, in general, the superposition of aleatory and epistemic uncertainties. Concerning the PAV system, the uncertainties in its main physical parameters are mostly due to the lack of fundamental physical knowledge in some of the phenomena occurring in tritium extraction process, often resulting in non-repeatable measurements. Considering e.g. the permeation properties of Nb, as also reported in [3], they should be a self-consistent set, in view of the relation linking the dissociation, recombination and solubility constants. However, new recent measurements of the permeability reported in [30] showed values orders of magnitude lower

Table 3
Range of variation for the PAV physical parameters.

Parameter	Min. value	Max. value	Mean log-value
K_r [$m^4/(mol\,s)$]	$3.94 \cdot 10^{-10}$	$6.02 \cdot 10^{-6}$	$4.87 \cdot 10^{-8}$
K_s^{PbLi} [$mol/(m^3\,Pa^{1/2})$]	$1.06 \cdot 10^{-3}$	$1.19 \cdot 10^{-1}$	$1.12 \cdot 10^{-2}$
K_s^{Nb} [$mol/(m^3\,Pa^{1/2})$]	$2.92 \cdot 10^{-2}$	$1.18 \cdot 10^{2}$	1.86
h_T [m/s]	$1.73 \cdot 10^{-5}$	$2.30 \cdot 10^{-3}$	$1.99 \cdot 10^{-4}$

than those computed analytically according to the permeability definition ($\Phi_{Nb} = K_s^{Nb} D_{Nb}$) in [31]. The latter used solubility [27,32] and diffusivity [33] values as measured by different laboratories, and therefore not necessarily self consistent, especially in view of the important conclusions of [30], highlighting that the measured values are strongly dependent on the surface oxidation status, driven by oxides that can form at room temperature and alter the results from one laboratory to the other. Therefore, the purpose of this section is twofold: (i) improving the physical understanding of these parameters by quantifying their cross-dependence and their impact on some relevant PAV output parameters and (ii) identifying the major contributors, among the input parameters, to the resulting uncertainty on the inlet and outlet tritium concentrations, $C_{PAV,in}$ and $C_{PAV,out}$, and, ultimately, on the PAV extraction efficiency η.

The physical parameters considered for the uncertainty propagation study and their range of variation are listed in Table 3. The minimum and maximum values of such parameters, evaluated at 500 °C (operative temperature of the PAV considered for the uncertainty propagation study), come from the disagreement between measurements of different laboratories (e.g. the value of K_s^{PbLi} found in literature can vary by two orders of magnitude depending on the empirical formulation considered), or, in the case of the mass transport coefficient h_T, from the uncertainty of the empirical formulation listed in Table 2 (for which an additional order of magnitude on the uncertainty, for both the upper and lower bound, is assumed to account for the fact that the correlation was developed for water, not PbLi).

5.1. The polynomial chaos expansion method

The considerable uncertainties in these parameters pose the question on how to effectively propagate them through the GETTHEM calculation. Their huge range of variation and the model non-linearities would suggest the adoption of a robust uncertainty propagation framework, like the one offered by a brute-force sampling technique. This approach consists in sampling the parameter space many times and evaluating the response of the physical model to the various samples. However, in spite of the computational efficiency of the GETTHEM code, the number of code evaluations would be cumbersome, due to the large number of samples needed to accurately map the input parameter space.

An efficient yet reliable alternative to brute-force methods is offered by non-intrusive Polynomial Chaos Expansion (PCE) methods [34]. This class of methods, which is very popular in the frame of uncertainty quantification and sensitivity analysis [34], allows to build a surrogate polynomial model that imitates the model of interest with a fair accuracy and a limited number of evaluations. Non-intrusive PCE has been extensively applied in many fields, including nuclear engineering [35–38].

The basic idea of this approach is expanding a stochastic model $\mathcal{M}$ in a series of orthogonal polynomials Ψ,

$$\mathcal{M}(\vec{s},t,\vec{p}) = \vec{y} = \sum_{k=0}^{\infty} \vec{a}_k(\vec{s},t)\Psi_k(\vec{p}) \approx \sum_{k=0}^{K} \vec{a}_k(\vec{s},t)\Psi_k(\vec{p}), \tag{10}$$

where $\vec{s}$ is the vector of the state variables (e.g., the space dependence), t is the time, $\vec{p}$ is the vector of stochastic parameters (in this case, the physical properties of the PAV), a_k is the kth expansion coefficient and K is the desired polynomial order. In this work, two popular methods are adopted for the evaluation of the projection coefficients $\vec{a}_k(\vec{s},t)$. The first one is the so-called *Non-Intrusive Pseudo-Spectral approach* (NISP), which consists of approximating the expansion coefficients through a quadrature rule [39], while the second one is the so-called *Non-Intrusive Point Collocation* (NIPC), which consists of evaluating $\vec{a}_k(\vec{s},t)$ by means of a least-square regression procedure [40].

5.2. The sampling strategy

If the input vector $\vec{p} \in \mathbb{R}^d$ is constituted by d independent random variables, the multivariate polynomials are expressed as a product of d independent polynomials. Hence, the number of coefficients to be evaluated grows exponentially with the number of dimensions. To mitigate this issue, known as *curse of dimensionality* [41], the *sparse grids* method [42] is often chosen. One advantage of this approach is that it can yield nested levels of points, i.e. the higher levels contain all the preceding, lower order ones, allowing to adaptively increase the number of points used to compute the quadrature or to perform the regression by re-using data from the previous levels.

Another delicate aspect concerning the input parameter space is its large variability: every input parameter spans at least two orders of magnitude. Due to this large variation, the samples are all assumed to follow a uniform distribution. Considering the large spread featuring these distributions and the non-linearity of the model, the samples are evaluated on a transformed input space, obtained by taking the logarithm of each input parameter, to ensure a uniform coverage of the various orders of magnitude. The log-transformation procedure is equivalent to drawing uniformly spaced samples on a logarithmic scale, as visible in Fig. 7(b), where a 2D view of the 4-dimensional space is provided by fixing two parameters.

Fig. 7 allows to appreciate another nice property of the sparse grid: thanks to Fig. 7(a), which shows a 3D view of the input space obtained by fixing $log(K_r^{Nb})$ to its mean value, it is possible to notice that, when also one of the other three parameters is fixed to its mean value, the 2D pattern of the grid, depicted in Fig. 7(b), is preserved. In particular, the points featuring the grid obtained by fixing two parameters out of four are exactly the same that would be obtained if the grid would be generated considering only a couple of parameters. This feature is very useful for a partial but systematic exploration of the input parameter space: the analysis may be initially carried out focusing on a subset of the parameter space, for instance involving only a couple of parameters, say h_T and K_s^{PbLi}. Afterwards, the inclusion of additional parameters in the uncertainty propagation study, say K_s^{Nb}, would only require to perform the model evaluations (i.e., the GETTHEM simulations) pertaining to the variations of this parameter with respect to its mean log-value (i.e., the points in Fig. 7(a) which are larger or smaller than the mean value of $log(K_s^{Nb})$, keeping the remaining parameter, i.e. K_r^{Nb}, at its mean log-value.

To better grasp the physical impact of the various inputs on the outputs of the GETTHEM model, the uncertainty propagation is first carried out for each couple of the four input parameters, exploiting the features of the sparse grids for minimising the number of model evaluations. Given the number of uncertain input parameters considered free to vary, Table 4 shows the number of samples, i.e. of GETTHEM simulations, needed for various levels of the sparse grid. Since the grid is nested, the actual number of new simulations required in a certain level is given by the difference between the number of points in that level and the number of points in the previous one.

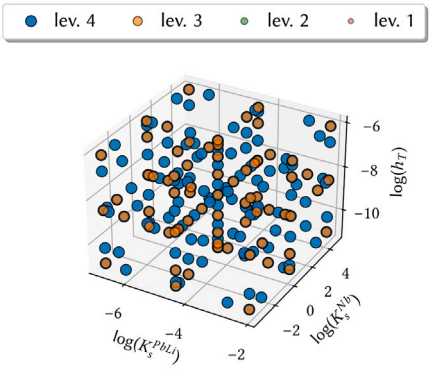

(a) 3D view of the sampled parameter space, obtained by fixing $log(K_r^{Nb})$ at its mean value.

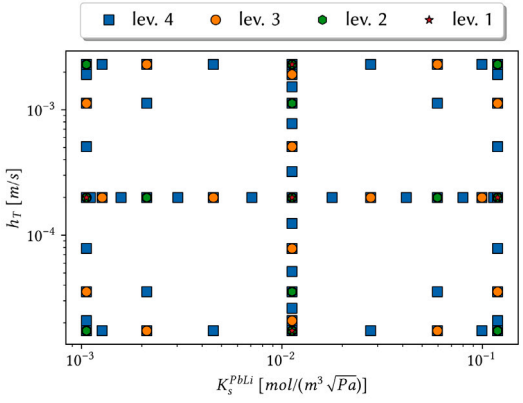

(b) 2D view of the sampled parameter space, obtained by fixing $log(K_r^{Nb})$ and $log(K_s^{Nb})$ at their respective mean values.

Fig. 7. Views of the sparse grid used to sample the input parameter space.

Table 4
Number of sample points required as a function of the grid level and the input space dimension.

# of uncertain parameter	Level 1	Level 2	Level 3	Level 4
2	5	13	29	65
3	7	25	69	177
4	9	41	137	401

5.3. Results of the 2D uncertainty propagation

The results obtained by considering each couple of parameters are presented and discussed in this Section, drawing some conclusions that could be useful to support the forthcoming experimental campaigns aiming at reducing the uncertainty on these input parameters.

5.3.1. PCE training and testing

The nested structure of the grid allows using a certain level to build the PCE model and then adopting the points belonging to the successive levels as validation points to check the performances of the polynomial fit. A preliminary analysis focusing on the type of PCE approach revealed that the NISP method offers roughly the same accuracy of the NIPC. However, the spectral projection requires specific points to carry out the quadrature, which limits the maximum polynomial order for the polynomial fit at the 4th degree, i.e. the maximum number of levels in the sparse grid. Since the NIPC does not require any rule for the sample points, this method is selected in the following to generate the surrogate fit for the model evaluations. All the PCE models have been generated with an *ad hoc* Python script that relies on the `chaospy` package [43]. As this preliminary uncertainty propagation study is focused on the tritium permeation model across the membrane (i.e. where the parameters with the largest uncertainty appear), the GETTHEM model adopted to generate the samples has been kept as simple as possible, thus modelling an open loop featuring the PAV model only, with fixed inlet conditions (PbLi pressure and temperature, and H-isotope partial pressure). Indeed, a closed loop model, such as that adopted in test cases I and II (see Section 4), could generate a back-propagation effect due to the recirculation of the PbLi from the outlet of the PAV (where H-isotope concentration is affected by the model uncertainty) to its inlet, causing a possible accumulation of tritium in the loop and therefore affecting the input (i.e. the tritium concentration at the PAV inlet) to the (uncertain) model.

Fig. 8 shows some curves obtained by fixing one of the two parameters considered in the generation of the 2D polynomial fit at its mean *log*-value. The circles and the stars represent the points adopted to carry out the regression process for the inlet and outlet concentrations, respectively. Analogously, the squares and the triangles represent the points adopted to test the performance of the regression model for the inlet and outlet concentrations, respectively. These graphs are very instructive from both physical and numerical points of view.

From a physical perspective, the scatter graphs can be interpreted as a One-At-a-Time sensitivity study [44], which yields the behaviour of the PAV model when only one parameter is varied at a time. First of all, it is possible to notice that, consistently with Sievert's law (see Eq. (5)) and the mentioned hypothesis of fixed inlet partial pressure, the inlet concentration only depends on K_s^{PbLi}, while the outlet concentration $C_{PAV,out}$ exhibits a non-linear dependence on all the parameters. In particular, it is very interesting to notice that this parameter tends to saturate towards the lower and upper limits of both K_r and K_s^{Nb}, i.e. where the curve exhibits two tails. Note that the x-axis on the graphs is given in a *log*-scale, meaning that in the saturation regions even significant variations in these two parameters may induce small or negligible variations in the outlet concentration. Since the PAV efficiency is proportional to the ratio $C_{PAV,out}/C_{PAV,in}$, it can be concluded that the variability of η due to the epistemic uncertainty in these parameters is expected to be very large for values far from the lower and upper limits.

From a numerical point of view, larger degrees in the polynomials increase the accuracy of the fit, except for low values of K_r and K_s^{Nb}. In these cases, see Figs. 8(b) and 8(c), the NIPC model always yields a value of $C_{PAV,out}$ larger than $C_{PAV,in}$, i.e. the resulting efficiency is negative. This physical inconsistency may be solved in a future work by increasing the number of points used to build the fit in the parameter space regions where the above-mentioned saturation effects in $C_{PAV,out}$ are significant. However, due to the preliminary and demonstrative nature of this uncertainty propagation study, this activity is left as a future work.

Fig. 9 shows the behaviour of the efficiency for the 2D parameter spaces defined by fixing each couple of parameters at a time to their mean *log*-values, allowing to visualise the dependence with respect to the various uncertain input parameters. A common feature to all these graphs is the fact that the largest values of the efficiency are placed in the corners, i.e. in correspondence of the upper or lower ranges of each parameter. In particular, high efficiencies can be obtained when K_r, K_s^{Nb} and h_T are all around their upper limit and K_s^{PbLi} is around its lower limit. Indeed, a high h_T enhances the mass transfer from the PbLi bulk to the fluid region near the membrane wall, while a large K_r value improves the recombination on the vacuum side (on the PbLi side the recombination is less important in view of the atomic dissolution of the H-isotope); in both cases, the extraction is enhanced. Large values of K_s^{PbLi} would instead reduce the permeated flux, thus a small K_s^{PbLi} improves the efficiency; a relatively high K_s^{Nb} would again improve the dissolution of the H-isotope in the membrane, enhancing its extraction from the fluid.

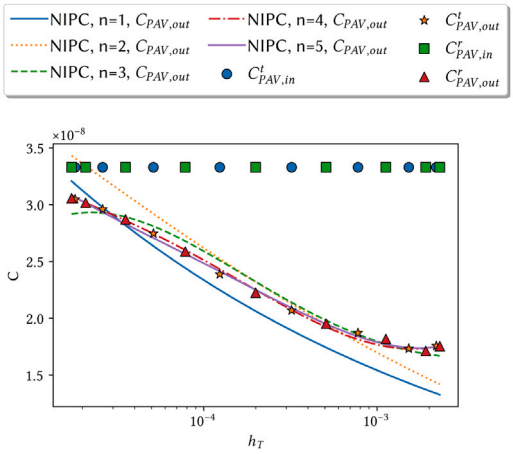

(a) 2D parameter space constituted by K_s^{PbLi} and h_T.

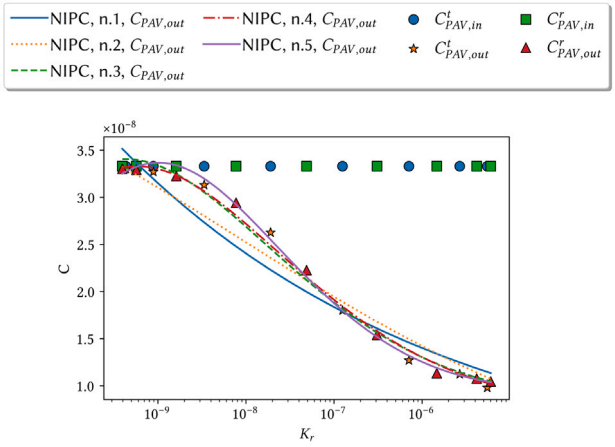

(b) 2D parameter space constituted by K_r and K_s^{PbLi}.

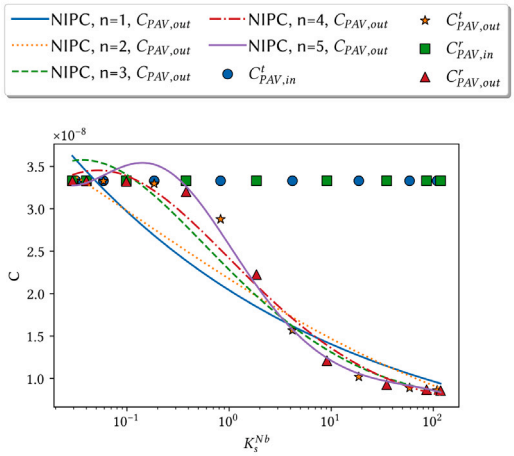

(c) 2D parameter space constituted by K_r and K_s^{Nb}.

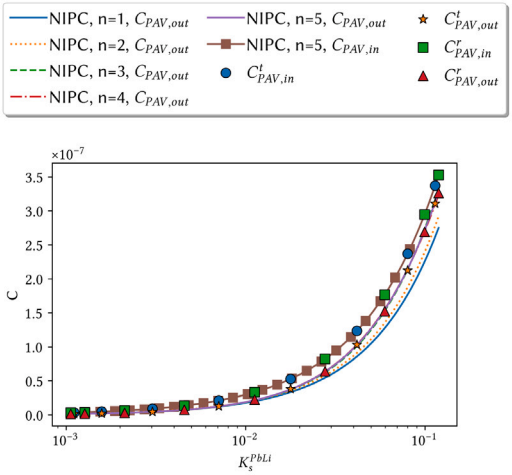

(d) 2D parameter space constituted by K_r^{Nb} and K_s^{PbLi}.

Fig. 8. Graphs showing 1D curves obtained by fixing one of the two parameters considered for the generation of the PCE model at its mean *log*-value.

Fig. 10 provides an overview of the relative error (in absolute value) on $C_{PAV,out}$ between the GETTHEM reference simulations and the NIPC model for the various 2D parameter spaces obtained by taking each couple of parameters at a time.

An inspection of these graphs helps to further corroborate the observation drawn previously about the saturation effect occurring for low values of K_s^{Nb} and K_r^{Nb}. From this perspective, the PCE models trained on the parameter spaces containing one of those two parameters feature the poorest accuracy (actually, the only model trained without any of the two shows the best accuracy, see Fig. 10(e)). Nevertheless, it should be acknowledged that, in most of the non-physical cases, the values of $C_{PAV,out}$ are only slightly larger than $C_{PAV,in}$ (< 3% with respect to $C_{PAV,in}$). Concerning the accuracy with respect to $C_{PAV,out}$, the models featured by the largest (> 15%) maximum relative errors are those defined over the spaces constituted by K_s^{Nb} and h_T and by K_r and h_T, followed by that constituted by K_s^{Nb} and K_r. The latter could be expected because of the poor performances of the PCE model near the upper and lower limits of K_s^{Nb} and K_r. Concerning the former two spaces, it should be noted that the behaviour (and the accuracy of the low-order fit) of h_T is qualitatively similar to that of K_s^{Nb} and K_r (while that of K_s^{PbLi} can be fitted well even by lower-order PCE models); therefore also the spaces involving the parameter h_T and K_s^{Nb} or K_r could be expected to show a lower accuracy. Except for some test cases showing a large relative error (between 12 and 25 %), most of the points are characterized by an error that is lower than 5 %. Since the objective of the PCE is to yield a surrogate (but computationally efficient) distribution of the PAV efficiency, the quality of the fit has been considered acceptable, despite the issue regarding possible negative values of this output parameter.

5.3.2. PCE results

After the training and testing phases, the PCE model can be finally applied as a computationally efficient surrogate of the GETTHEM model for the generation of a sample Probability Density Function (PDF) of the PAV efficiency η.

Fig. 11 represents the various PDFs for η obtained by considering the different couples of uncertain physical parameters. The sample PDFs are simply built by running the 5th order NIPC model a large number of times (in this case, 10^4) and gathering the outcomes. Since some efficiency values might be negative, another PDF, in orange, is superimposed to the original one (in light blue), by imposing $\eta = 0$ when $C_{PAV,out} > C_{PAV,in}$. This operation is justified by the fact that the efficiency tends to zero for small values of K_r and K_s^{Nb}, as previously observed.

By inspection of this figure, it can be easily appreciated that in general the PDF shows two peaks around the minimum and maximum values of η, while the probability of getting η in the interval (0,1) is rather uniform. The spread of the distributions is very large. The

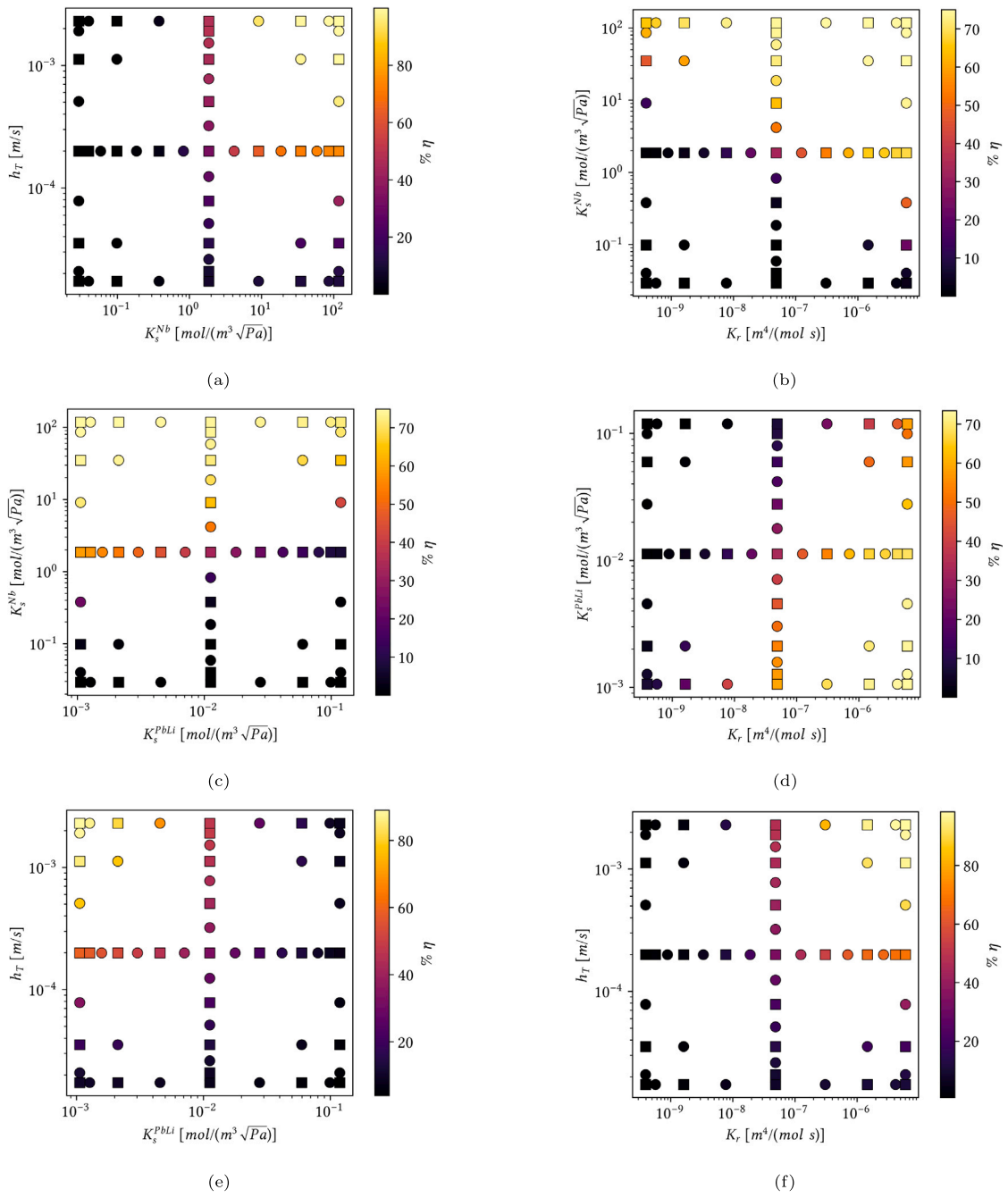

Fig. 9. Efficiency behaviour with respect to each couple of free parameters considered in the regression generation process. The colour is proportional to the efficiency magnitude; the squares indicate the training points while the circles represent the test points. (For interpretation of the references to colour in this figure legend, the reader is referred to the web version of this article.)

general behaviour of these PDFs points out that the uncertainty on the input physical parameters leads to an unacceptable uncertainty on the PAV efficiency, thus asking for an improvement in their experimental evaluation.

Another useful property of the PCE method is that it allows to easily retrieve the first order Sobol's indices, which can be defined as

$$S_i = \frac{\sigma_i^2}{\sigma_{TOT,R}^2}, \tag{11}$$

where σ_i^2 is the variance due to the i^{th} parameter, $\sigma_{TOT,R}^2$ is the total variance on the output response R and S_i is the Sobol's index quantifying the fraction of the total variance due to the i^{th} parameter alone. As such, Sobol's indices can be adopted as global indicators of the model sensitivity to a certain input parameter considering the whole parameter space [45]. The Sobol's indices are normalised,

$$\sum_{i=1}^{d} \frac{\sigma_i^2}{\sigma_{TOT,R}^2} + \sum_{i<j}^{d} \frac{\sigma_{ij}^2}{\sigma_{TOT,R}^2} + \cdots + \frac{\sigma_{12\ldots d}^2}{\sigma_{TOT,R}^2} = 1, \tag{12}$$

thus also the fraction of output variance due to the interaction of one or more parameters, e.g., that due to the interaction between the i^{th} and j^{th} parameters, is accounted for.

Table 5 reports the Sobol's indices computed for the different 2D input spaces considered in the analysis for the outlet concentration. As expected on a physical ground, $C_{PAV,in}$ is only sensitive to K_s^{PbLi}, therefore it was not included in the table, while $C_{PAV,out}$ depends on all the four parameters. In particular, it is interesting to observe that the

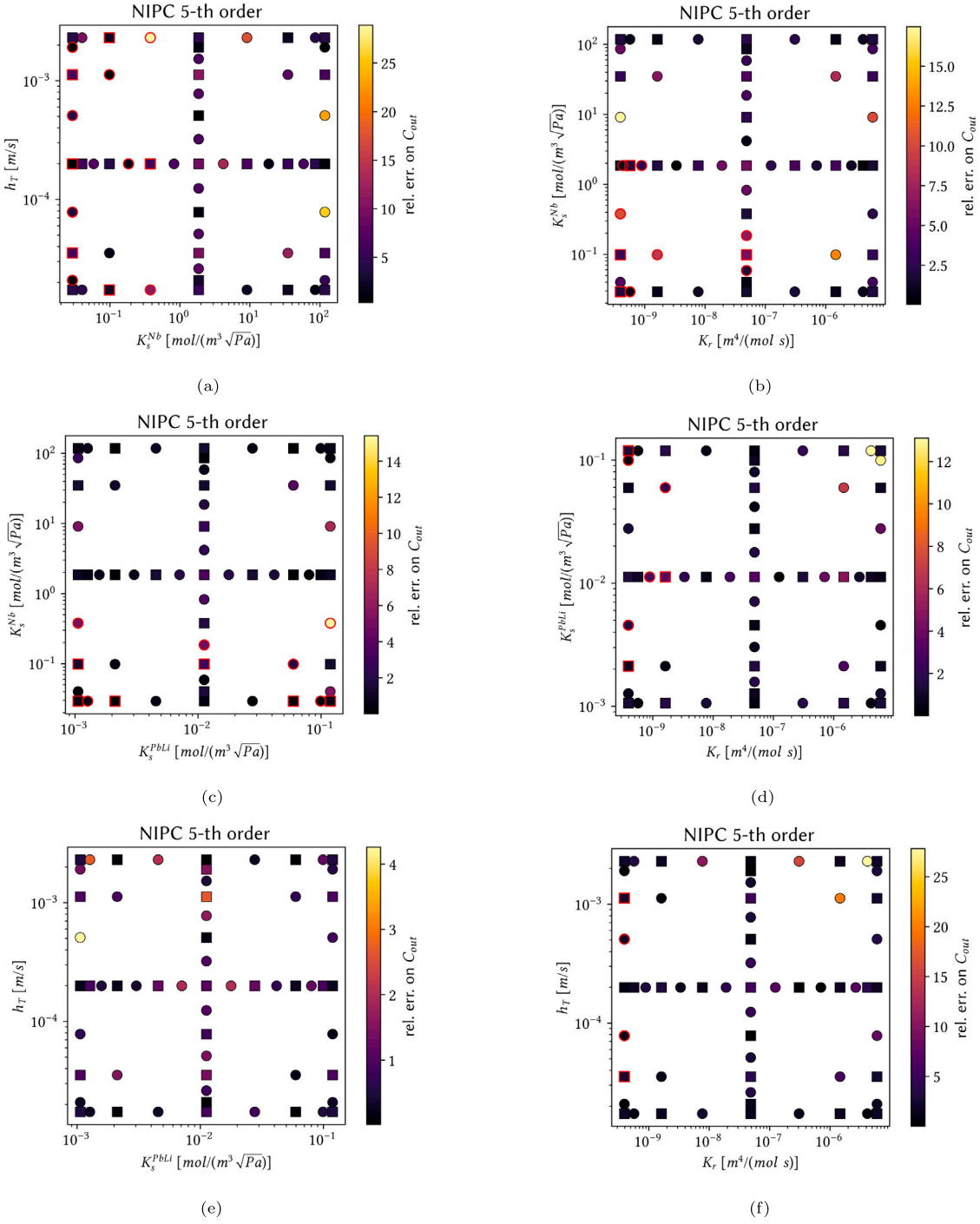

Fig. 10. Relative errors between reference and NIPC model with respect to each couple of free parameters considered in the regression generation process. The colour is proportional to the relative error; the squares indicate the training points while the circles represent the test points. The markers with a red edge indicate the non-physical cases characterized by $C_{PAV,out} > C_{PAV,in}$. (For interpretation of the references to colour in this figure legend, the reader is referred to the web version of this article.)

cross-variances between K_s^{PbLi} and K_r, as well as that between K_s^{PbLi} and K_s^{Nb}, are negligible (as it can be also observed in relative terms in Figs. 9(c) and 9(d)), suggesting that the recombination and solubility constants of Nb are rather independent on K_s^{PbLi}. The fact that the two solubility constants are independent on each other is quite obvious, being two different material. The small dependence of the recombination constant on the K_s^{PbLi} could be due to the fact that being the hydrogen isotopes dissolved in atomic form in the PbLi, a real recombination (that could be related to the solubility constant in the PbLi) is not needed on the PbLi side. Also the mutual interaction between h_T and K_s^{PbLi} is quite small. These values of the mutual interactions can be explained by noticing that the dominant contribution (≥∼ 90%) in the total variance is always due to the PbLi solubility constant. As it can be observed also in Fig. 8, the variation in both $C_{PAV,in}$ and $C_{PAV,out}$ due to this parameter is the largest, compared to the other variables.

Concerning the other couples, the mutual interaction of K_s^{Nb} and K_r amounts to 6 % of the total variance, which is still rather small. On the contrary, when h_T is coupled with K_r or K_s^{Nb}, the mutual interaction becomes important. The physical interaction between them can be related to the fact that h_T (on the PbLi side) and the K_r and K_s^{Nb} (on the membrane side) strongly influence the hydrogen isotope transport close to the membrane wall, and therefore the local gradients there.

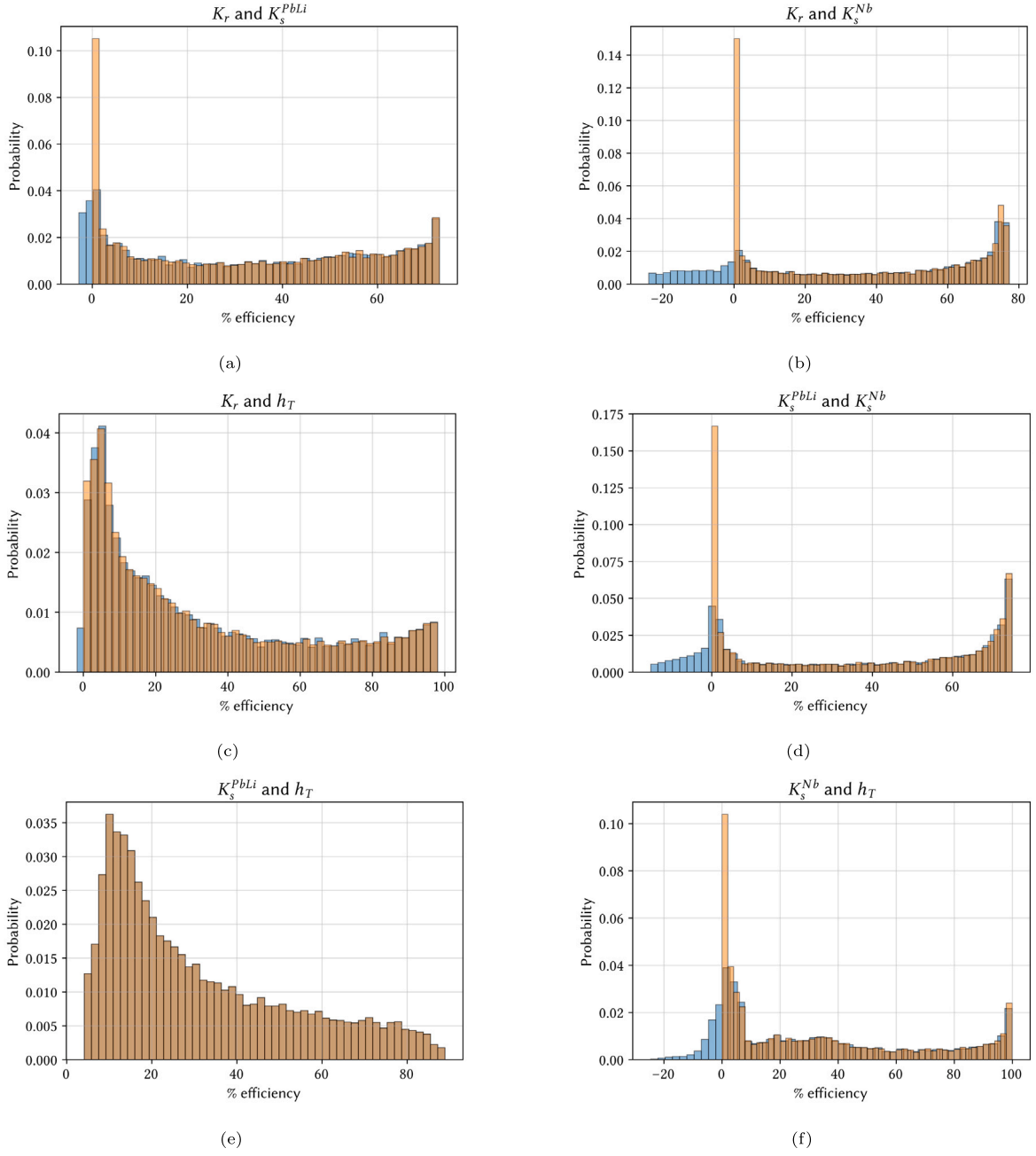

Fig. 11. Sample probability density function for the PAV efficiency considering the different parameter spaces. The PDF obtained imposing $\eta = 0$ when $C_{PAV,in} < C_{PAV,out}$ is reported in orange, superimposed to the original one (in light blue). (For interpretation of the references to colour in this figure legend, the reader is referred to the web version of this article.)

6. Conclusions and perspective

The PbLi loop model available in the GETTHEM system-level code, already including models for the generation, transport and removal of Activated Corrosion Products as Dispersed Materials (DM), has been extended to include the transport and removal of hydrogen isotopes and helium from the PbLi alloy.

The mass balance equation along the PbLi flow is solved for the above-mentioned species, assumed to be found in the working fluid in trace concentrations only. A recently-developed model for the hydrogen mass transport phenomena in the radial direction of the PAV channels (permeation through a niobium membrane driven by the hydrogen partial pressure difference between the two sides of the membrane) capturing the permeation has been implemented for the TERS in GETTHEM. The permeation model is able to address both diffusion-limited and surface-limited permeation regimes, depending on the input permeation parameters and operating conditions. In perspective, the liquid-limited permeation regime, discussed in [46], will also be investigated. The new implementation has been successfully verified with an order-of-accuracy test, adopting the method of the manufactured solution.

Two simple test cases for the PbLi have been simulated, adopting the configuration proposed for the PAV mock-up. The capability of the model to compute (i) the concentration of different DM species at the same time (hydrogen and helium in this case) in different locations of the PbLi loop, and (ii) the H-isotope extraction along the PAV channels has been demonstrated during different possible transients.

In view of the large uncertainty on the model physical parameters, a preliminary uncertainty propagation study has also been carried out

Table 5
Sobol's first order sensitivity indices for the PAV outlet concentration $C_{PAV,out}$.

1st parameter	2nd parameter	Interaction
K_r	K_s^{PbLi}	
5.33%	94.32%	0.35%
K_r	K_s^{Nb}	
21.86%	72.05%	6.09%
K_s^{PbLi}	h_T	
96.30%	2.19%	1.51%
K_s^{Nb}	h_T	
43.11%	21.70%	35.19%
K_s^{PbLi}	K_s^{Nb}	
89.08%	10.59%	0.34%
K_r^{Nb}	h_T	
46.49%	23.61%	29.90%

with the Polynomial Chaos Expansion technique, to assess the effect of the different empirical formulations available for the permeation parameters on the computed outlet H-isotope concentration. It turned out that the uncertainty on the input parameters leads to an unacceptable uncertainty on the PAV efficiency, suggesting a need for an improvement in their experimental evaluation. In particular, K_s^{PbLi} is uncorrelated to both K_r and K_s^{Nb}, and shows the dominant contribution in the total variance; therefore, it is a good candidate to be the first property asking for better accuracy. However, as h_T shows a strong mutual interaction with K_r and K_s^{Nb}, also a reduction of its uncertainty could lead to important benefits on the overall model accuracy.

In perspective, the qualification of the model will be completed through a validation against experimental data coming from the PAV mock-up tests performed at the TRIEX-II facility. Moreover, the model will be extended to include part of the vacuum circuit (secondary side of the PAV extractor) and realistic tritium generation models, and the effect of the PAV channels entrance region on the transport of hydrogen isotopes in PbLi will be investigated. Finally, the uncertainty propagation study will also be extended varying all the parameters simultaneously.

CRediT authorship contribution statement

Roberto Bonifetto: Conceptualization, Methodology, Supervision, Writing – review & editing. **Nicolò Abrate:** Methodology, Formal analysis, Writing – original draft. **Antonio Froio:** Conceptualization, Methodology, Supervision, Writing – review & editing. **Fabrizio Lisanti:** Validation, Software, Writing – original draft. **Francesca Papa:** Project administration. **Marco Utili:** Project administration, Funding acquisition. **Alessandro Venturini:** Project administration, Funding acquisition.

Declaration of competing interest

The authors declare the following financial interests/personal relationships which may be considered as potential competing interests: Roberto Bonifetto reports financial support was provided by Euratom Research and Training Programme.

Data availability

The authors are unable or have chosen not to specify which data has been used.

Table A.1
Shapes of the manufactured solutions applied to the set of variables for the verification. $t_0 = 30$ s, $B = 10$, $\omega = 0.5$, $\Phi = \pi/4$; t is the time variable.

Variable	Unit	Shape
$C_T(x,t)$	kg_T/kg_{PbLi}	$B\frac{MM_T}{\rho_{PbLi}(x)}\left[1+\sin\left(\frac{\pi x}{L}\right)\right]\left(1+\exp\left(-\frac{t}{t_0}\right)\right)$
$J_T(x)$	$mol/(m^2\,s)$	$B\left[\frac{1}{2}\sin\left(\frac{\pi x}{L}\right)+1\right]$
$C_{T,l}(x)$	kg_T/kg_{PbLi}	$\frac{MM_T}{\rho_{PbLi}(x)}\frac{B}{2}\exp\left(\frac{x}{L}\right)$
$\widetilde{C}_{T,win}(x)$	$mol_T/(m^3_{PbLi})$	$\frac{B}{4}\exp\left(\frac{x}{L}\right)$
$\widetilde{C}_{T,wout}(x)$	$mol_T/(m^3_{PbLi})$	$B\left[\frac{1}{2}\sin\left(\frac{\pi x}{L}\right)+2\right]$
$p_{T,l}(x)$	Pa	$B\sin\left(\frac{\omega x}{L}+\Phi\right)$

Acknowledgements

This work has been carried out within the framework of the EUROfusion Consortium, funded by the European Union via the Euratom Research and Training Programme (Grant Agreement No 101052200 – EUROfusion). Views and opinions expressed are however those of the author(s) only and do not necessarily reflect those of the European Union or the European Commission. Neither the European Union nor the European Commission can be held responsible for them.

Appendix. Verification

The verification of the Modelica implementation of the 1D transport and permeation models introduced in Section 2 is reported here: the Order-of-Accuracy (OoA) test has been carried out, adopting the method of the manufactured solution (MMS) [47]. This method was chosen because, with respect to other verification methods, e.g. the benchmark against a simplified analytical solution, it does not require any simplification of the existing model or assumptions on the model parameters. The MMS is used to verify the correct implementation of the discretization procedure for a set of equations containing at least one Partial Differential Equation (PDE). It consists in choosing an arbitrary ("manufactured") solution and substitute it in the original PDE(s) to compute analytically the fictitious source terms. The latter are then added to the discretized set of PDEs, and the convergence of the numerical solution to the manufactured one is studied (e.g. varying the mesh size), to assess that the discretization error changes at the expected rate.

In this work, the MMS has been applied to a set of 6 equations describing the transport and permeation phenomena, presented in Section 2.2, adding the fictitious source terms $Q_{1,\dots,6}$

$$\begin{cases} \frac{\partial(\rho_{PbLi}(x)C_T(x))}{\partial t} + \frac{\partial(\rho_{PbLi}(x)C_T(x))v}{\partial x} = -J_T(x)\frac{2}{r_{in}}MM_T + Q_1 \\ J_T(x) = h_T\left(C_T(x) - C_{T,l}(x)\right)\frac{\rho_{PbLi}(x)}{MM_T} + Q_2 \\ C_{T,l}(x)\frac{\rho_{PbLi}(x)}{MM_T} = K_s^{PbLi}\sqrt{p_{T,l}(x)} + Q_3 \\ J_T(x) = D_{Nb}(x)\frac{\widetilde{C}_{T,w,in}(x) - \widetilde{C}_{T,w,out}(x)}{r_{in}\log\left(\frac{r_{out}}{r_{in}}\right)} + Q_4 \\ J_T(x) = K_d^{Nb}(x)p_{T,l}(x) - K_r^{Nb}(x)\widetilde{C}^2_{T,w,in}(x) + Q_5 \\ J_T(x) = 2\frac{r_{out}}{r_{in}}K_r^{Nb}(x)\widetilde{C}^2_{T,w,out}(x) - \frac{1}{2}\frac{r_{out}}{r_{in}}K_d^{Nb}(x)p_{vc} + Q_6 \end{cases} \quad (A.1)$$

where the mass balance in Eq. (1) has been expressed in terms of the bulk concentration knowing that $\rho_T = \rho_{PbLi}C_T$. Note that the method used to discretize the spacial derivatives is the same used in Section 2.2. Imposing the manufactured solutions listed in Table A.1 (chosen among any C^∞ functions) in the set of Eqs. (A.1), the fictitious source terms $Q_{1,\dots,6}$ to be implemented in the model are found.

The convergence study was performed on a trivial test case where the PAV channel model implementing the tritium mass transport is placed between a mass flow source and a sink. For the pipe model, a length $L = 40$ m was assumed, while for the membrane an inner radius

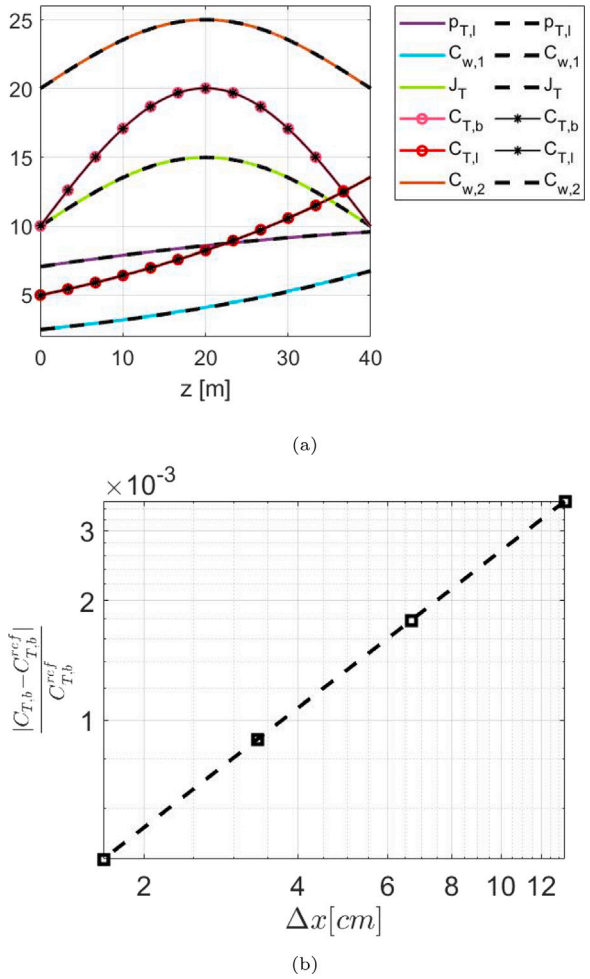

Fig. A.1. Results of the verification and OoA analysis: (a) shape of the numerical solutions (dashed and symbolic lines) computed imposing the fictitious source terms, compared to the manufactured solution (in solid and symbolic lines), and (b) OoA analysis for the tritium concentration at the PAV outlet, where the expected OoA is shown by the dashed line.

$r_{in} = 4.6$ mm and an outer radius $r_{out} = 5$ mm were adopted, as well as a temperature $T = 330$ °C and mass flow rate $\dot{m} = 1$ kg/s for the PbLi flow. Fig. A.1 shows the results of the verification and convergence analysis. The relative error (evaluated at the outlet of the PAV channel) on the computed solution for the concentration (shown in Fig. A.1(b)) halves when the Δx is halved, resulting in an OoA of the 1st order, as expected considering the FV approximation with an upwind scheme [48].

References

[1] A.J.H. Donné, W. Morris, X. Litaudon, C. Hidalgo, D. McDonald, H. Zohm, E. Diegele, A. Möslang, K. Nordlund, G. Federici, P. Sonato, C. Waldon, D. Borba, P. Helander, European Reasearch Roadmap to the Realisation of Fusion Energy, EUROfusion Consortium, 2018, ISBN 978–3–00–061152–0.

[2] P. Arena, A. Del Nevo, F. Moro, S. Noce, R. Mozzillo, V. Imbriani, F. Giannetti, F. Edemetti, A. Froio, L. Savoldi, A. Tassone, F. Roca Urgorri, P.A. Di Maio, I. Catanzaro, G. Bongiovì, The DEMO Water-Cooled Lead-Lithium breeding blanket: Design status at the end of the pre-conceptual design phase, Appl. Sci. 11 (24) (2021) 11592, http://dx.doi.org/10.3390/app112411592.

[3] R. Bonifetto, M. Utili, D. Valerio, R. Zanino, Conceptual design of a PAV-based tritium extractor for the wcll breeding blanket of the EU DEMO: Effects of surface-limited vs. diffusion-limited modeling, Fusion Eng. Des. 167 (2021) 112363, http://dx.doi.org/10.1016/j.fusengdes.2021.112363.

[4] D. Valerio, R. Bonifetto, M. Utili, R. Zanino, Effects of surface-limited vs. diffusion-limited modeling on the conceptual design of a PAV-based TERS for the WCLL blanket of the EU DEMO, in: Presented At SOFT2020, 2020.

[5] F. Papa, M. Utili, A. Venturini, G. Caruso, L. Savoldi, R. Bonifetto, D. Valerio, A. Allio, A. Collaku, M. Tarantino, Engineering design of a permeator against vacuum mock-up with niobium membrane, Fusion Eng. Des. 166 (2021) 112313, http://dx.doi.org/10.1016/j.fusengdes.2021.112313.

[6] A. Froio, C. Bachmann, F. Cismondi, L. Savoldi, R. Zanino, Dynamic thermal-hydraulic modelling of the EU DEMO HCPB breeding blanket cooling loops, Prog. Nucl. Energy 93 (2016) 116–132, http://dx.doi.org/10.1016/j.pnucene.2016.08.007.

[7] A. Froio, F. Casella, F. Cismondi, A. Del Nevo, L. Savoldi, R. Zanino, Dynamic thermal-hydraulic modelling of the EU DEMO WCLL breeding blanket cooling loops, Fusion Eng. Des. 124 (2017) 887–891, http://dx.doi.org/10.1016/j.fusengdes.2017.01.062.

[8] M. Utili, C. Alberghi, L. Candido, F. Papa, M. Tarantino, A. Venturini, TRIEX-II: an experimental facility for the characterization of the tritium extraction unit of the WCLL blanket of ITER and DEMO fusion reactors, Nucl. Fusion 62 (6) (2022) 066036.

[9] F. Papa, A. Venturini, D. Martelli, M. Utili, Tritium extraction from lithium–lead eutectic alloy: Experimental characterization of a permeator against vacuum mock-up at 450 °C, Energies 16 (7) (2023) 3022.

[10] E. Carella, C. Moreno, EcosimPro detailed document package, 2015, EFDA_D_2L3JCZ v2.0.

[11] F.R. Urgorri, C. Moreno, E. Carella, J. Castellanos, A. Del Nevo, Á. Ibarra, Preliminary system modeling for the EUROfusion water cooled lithium lead blanket, Fusion Sci. Technol. 71 (3) (2017) 444–449.

[12] F. Urgorri, C. Moreno, E. Carella, D. Rapisarda, I. Fernández-Berceruelo, I. Palermo, A. Ibarra, Tritium transport modeling at system level for the EUROfusion dual coolant lithium-lead breeding blanket, Nucl. Fusion 57 (11) (2017) 116045.

[13] F. Franza, A. Ciampichetti, I. Ricapito, M. Zucchetti, A model for tritium transport in fusion reactor components: The FUS-TPC code, Fusion Eng. Des. 87 (4) (2012) 299–302.

[14] F. Franza, Tritium Transport Analysis in Advanced Sodium-Cooled Fast Reactors, (Master's thesis), Politecnico di Torino, Italy, 2011.

[15] A. Santucci, A. Ciampichetti, D. Demange, F. Franza, S. Tosti, Tritium migration in HCLL and WCLL blankets: impact of tritium solubility in liquid Pb-17Li, IEEE Trans. Plasma Sci. 42 (4) (2014) 1053–1057.

[16] F. Casella, A. Leva, Modelica open library for power plant simulation: design and experimental validation, in: Proceedings of the 3rd International Modelica Conference, 3–4 November 2003, Linköping, Sweden, 2003, pp. 41–50.

[17] F. Lisanti, P. Arena, R. Bonifetto, A. Froio, F.A. González Hernández, G.A. Spagnuolo, R. Zanino, Modeling the transport of activated corrosion products in the WCLL PbLi loop for ITER and the EU DEMO with the GETTHEM code, IEEE Access 11 (2023) 22614–22628, http://dx.doi.org/10.1109/ACCESS.2023.3252905.

[18] F. Casella, M. Otter, K. Proelss, C. Richter, H. Tummescheit, The Modelica Fluid and Media library for modeling of incompressible and compressible thermo-fluid pipe networks, in: Proceedings of the 5th International Modelica Conference, 4-5 September 2006, Wien, 2006, pp. 631–640.

[19] R. Franke, F. Casella, M. Sielemann, K. Proelss, M. Otter, M. Wetter, Standardization of thermo-fluid modeling in Modelica.Fluid, in: Proceedings of the 7th Modelica Conference, 20-22 September 2009, Como, Italy, 2009.

[20] V. D'Auria, S. Dulla, P. Ravetto, L. Savoldi, M. Utili, R. Zanino, Tritium extraction from lithium-lead in the EU DEMO blanket using permeator against vacuum, Fusion Sci. Technol. 71, no.4 (2017) 537–543, http://dx.doi.org/10.1080/15361055.2017.1291252.

[21] V. D'Auria, S. Dulla, P. Ravetto, L. Savoldi, M. Utili, R. Zanino, Design of a permeator-against-vacuum mock-up for the tritium extraction from PbLi at low speed, Fusion Eng. Des. 121 (2017) 198–203, http://dx.doi.org/10.1016/j.fusengdes.2017.07.006.

[22] P.W. Humrickhouse, B.J. Merrill, Vacuum permeator analysis for extraction of tritium from DCLL blankets, Fusion Sci. Technol. 68 (2) (2015) 295–302.

[23] M.A. Pick, K. Sonnenberg, A model for atomic hydrogen-metal interactions–application to recycling, recombination and permeation, J. Nucl. Mater. 131 (1985) 208–220.

[24] I. Ali-Khan, K.J. Dietz, F.G. Waelbroeck, P. Wienhold, The rate of hydrogen release out of clean metallic surfaces, J. Nucl. Mater. 76–77 (1978) 337–343.

[25] E. Mas de les Valls, L. Sedano, L. Batet, I. Ricapito, A. Aiello, O. Gastaldi, F. Gabriel, Lead–lithium eutectic material database for nuclear fusion technology, J. Nucl. Mater. 376 (2008) 353–357.

[26] Y.C. Chan, E. Veleckis, A thermodynamic investigation of dilute solutions of hydrogen in liquid Li-Pb alloys, J. Nucl. Mater. 122 & 123 (1984) 935–940.

[27] S. Steward, Isotope effects in solutions of hydrogen and deuterium in niobium, J. Chem. Phys. 63 (2) (1975) 975–979.

[28] P. Harriot, R.M. Hamilton, Solid-liquid mass transfer in turbulent pipe flow, Chem. Eng. Sci. 20, no.12 (1965) 1073–1078.

[29] M. Yamawaki, N. Chitose, V. Bandurko, K. Yamaguchi, Impact of surface phenomena in metals on hydrogen isotope permeation, Fusion Eng. Des. 28 (1995) 125–130.

[30] M. Malo, B. Garcinuño, D. Rapisarda, Experimental refutation of the deuterium permeability in vanadium, niobium and tantalum, Fusion Eng. Des. 146 (2019) 224–227.

[31] S.A. Steward, Review of Hydrogen Isotope Permeability Through Materials, lawrence livermore national laboratory, 1984, Ucrl-53441.
[32] E. Veleckis, R.K. Edwards, Thermodynamic properties in the systems vanadium-hydrogen, niobium-hydrogen, and tantalum-hydrogen, J. Phys. Chem. 73 (3) (1969) 683–692.
[33] J. Volkl, G. Alefeld, Diffusion in Solids: Recent Developments, by AS Nowick and JJ Burton, Chap 6, Academic Press, New York, 1975.
[34] D. Xiu, G.E. Karniadakis, The Wiener–Askey polynomial chaos for stochastic differential equations, SIAM J. Sci. Comput. 24 (2) (2002) 619–644, URL https://doi.org/10.1137/S1064827501387826.
[35] P. Turati, A. Cammi, S. Lorenzi, N. Pedroni, E. Zio, Adaptive simulation for failure identification in the advanced lead fast reactor European demonstrator, Prog. Nucl. Energy 103 (2018) 176–190.
[36] M. Santanoceto, M. Tiberga, Z. Perkó, S. Dulla, D. Lathouwers, Preliminary uncertainty and sensitivity analysis of the molten salt fast reactor steady-state using a polynomial chaos expansion method, Ann. Nucl. Energy 159 (2021) 108311.
[37] N. Abrate, S. Dulla, N. Pedroni, A non-intrusive reduced order model for the characterisation of the spatial power distribution in large thermal reactors, Ann. Nucl. Energy 184 (2023) 109674.
[38] A. Aimetta, N. Abrate, S. Dulla, A. Froio, A nonintrusive nuclear data uncertainty propagation study for the ARC fusion reactor design, Nucl. Sci. Eng. 197 (2023) 2192–2216, http://dx.doi.org/10.1080/00295639.2022.2153638.
[39] S. Avasarala, D. Subramani, A non-Gaussian Bayesian filter for sequential data assimilation with non-intrusive polynomial chaos expansion, Internat. J. Numer. Methods Engrg. 122 (23) (2021) 7156–7181.
[40] S. Hosder, R.W. Walters, M. Balch, Point-collocation nonintrusive polynomial chaos method for stochastic computational fluid dynamics, AIAA J. 48 (12) (2010) 2721–2730.
[41] R. Bellman, Dynamic Programming, in: Rand Corporation research study, Princeton University Press, 1957, URL https://books.google.it/books?id=wdtoPwAACAAJ.
[42] S.A. Smolyak, Quadrature and interpolation formulas for tensor products of certain classes of functions, Dokl. Akad. Nauk SSSR 148 (5) (1963) 1042–1045.
[43] J. Feinberg, H.P. Langtangen, Chaospy: An open source tool for designing methods of uncertainty quantification, J. Comput. Sci. 11 (2015) 46–57, URL https://www.sciencedirect.com/science/article/pii/S1877750315300119.
[44] D.G. Cacuci, M. Ionescu-Bujor, A comparative review of sensitivity and uncertainty analysis of large-scale systems—II: statistical methods, Nucl. Sci. Eng. 147 (3) (2004) 204–217.
[45] B. Sudret, Global sensitivity analysis using polynomial chaos expansions, Reliab. Eng. Syst. Saf. 93 (7) (2008) 964–979, URL https://www.sciencedirect.com/science/article/pii/S0951832007001329.
[46] C. Alberghi, L. Candido, M. Utili, M. Zucchetti, Development of new analytical tools for tritium transport modelling, Fusion Eng. Des. 177 (2022) 113083.
[47] C.J. Roy, Review of code and solution verification procedures for computational simulation, J. Comput. Phys. 205 (1) (2005) 131–156.
[48] A. Quarteroni, Numerical Models for Differential Problems, first ed., Springer Milano, 2013, http://dx.doi.org/10.1007/978-88-470-1071-0.